UNIVERSITY OF LEEDS

This is a repository copy of *Trends in the local Hadley and local Walker circulations*.

White Rose
university consortium
Universities of Leeds, Sheffield & York

eprints@whiterose.ac.uk
https://eprints.whiterose.ac.uk/

RESEARCH ARTICLE

Key Points:
- Local Hadley circulation shifted southward from Africa to Central Pacific
- Local Hadley circulation intensified over the Americas and the Atlantic
- Local Walker circulations weakened in all ocean basins

Correspondence to:
J. Schwendike,
juliane.schwendike@monash.edu.au

Trends in the local Hadley and local Walker circulations

Juliane Schwendike[1], Gareth J. Berry[1], Michael J. Reeder[1], Christian Jakob[1,2], Pallavi Govekar[1,3], and Richard Wardle[4]

[1]School of Earth, Atmosphere and Environment, Monash University, Clayton, Victoria, Australia, [2]ARC Centre of Excellence for Climate System Science, Monash University, Clayton, Victoria, Australia, [3]School of Earth Sciences, Melbourne University, Melbourne, Victoria, Australia, [4]Bureau of Meteorology, Brisbane, Queensland, Australia

Abstract The linear trend in the local Hadley and Walker circulations from 1979 to 2009 is calculated. These local circulations are defined through a decomposition of the vertical mass flux into its zonal and meridional components. Defining the local circulation this way ensures that the two orthogonal circulations (the local Hadley and Walker circulations) sum to the original circulation even after averaging the circulations regionally. Large regional differences in changes in the local Hadley and Walker circulations over a 31 year period are found. For example, the local Hadley circulation has shifted southward over Africa, the Maritime Continent, and the western and central Pacific by about 1°. Over the Americas and the Atlantic the local Hadley circulation has strengthened by about 1–5%. The zonal component of the vertical mass flux has increased by about 10–20% in the tropics over all continents and decreased over the adjacent oceans by about 10–20%. Although the local Walker circulations in the Indian Ocean and the Atlantic have weakened, the circulation in the Pacific has changed little (about 1–2%). The local Walker circulations in all ocean basins have shifted westward by about 1–2° on average.

1. Introduction

The Hadley and Walker circulations are the largest overturning circulations in the atmosphere covering about one third of the globe. Although there is agreement in the literature that the tropics, defined by the Hadley circulation, have expanded [e.g., *Seidel and Randel*, 2007; *Lu et al.*, 2007; *Hu and Fu*, 2007; *Seidel et al.*, 2008; *Johanson and Fu*, 2009; *Fu and Lin*, 2011; *Liu et al.*, 2012; *Nguyen et al.*, 2013; *Quan et al.*, 2014], there is disagreement on the rate of this expansion. The trends for the northern and southern cells are different and range from 0.1 to over 1.0° latitude per decade [*Lucas et al.*, 2013].

These trends in the Hadley circulation have been based on changes in the tropopause height [e.g. *Seidel and Randel*, 2007; *Lu et al.*, 2007; *Davis and Rosenlof*, 2012] and the mass stream function, or by changes in the position of the jet stream [e.g., *Davis and Rosenlof*, 2012; *Davis and Birner*, 2013] in reanalyses data. Similar calculations have been based on satellite-based methodologies [e.g., *Fu et al.*, 2006; *Hu and Fu*, 2007; *Seidel et al.*, 2008; *Johanson and Fu*, 2009; *Fu and Lin*, 2011; *Stachnik and Schumacher*, 2011; *Allen et al.*, 2012; *Nguyen et al.*, 2013; *Hu and Fu*, 2013].

The Coupled Model Intercomparison Project phase 3 models shows a poleward expansion of the Hadley circulation by about 1–2° over the 21st century and a decrease in the intensity of both the Hadley and the Walker circulations due to increased greenhouse gas concentrations [e.g., *Lu et al.*, 2007; *Chen et al.*, 2002; *Held and Soden*, 2006; *Gastineau et al.*, 2008]. *Lucas et al.* [2013], however, points out that there is no consensus on the dynamical mechanism behind the tropical expansion.

Trends in the Walker circulation for different climate scenarios mainly show a weakening [*Tanaka et al.*, 2004; *Vecchi et al.*, 2006; *Vecchi and Soden*, 2007; *Deser and Phillips*, 2009; *Gastineau et al.*, 2009; *DiNezio et al.*, 2013; *Bayr et al.*, 2014]. The weakening of the large-scale tropical circulation leads to a reduced transport of water vapor from the boundary layer to the free atmosphere [*Held and Soden*, 2006], thereby affecting the global water cycle. *Bayr et al.* [2014] found recently that the Walker circulation in the Pacific is also shifting to the west.

Although zonally and meridionally averaged circulations provide very useful, compact representations of the principal overturning circulations, the averaging masks the huge spatial variability in these circulations at the local or regional scale. The local meridional overturning circulation in the tropics, the zonal average of which is the Hadley circulation, is not uniform around the globe, but differs from continent to continent and in each

ocean basin [e.g. *Goswami et al.*, 1999; *Gedney and Valdes*, 2000, and *Chen et al.*, 2014; *Schwendike et al.*, 2014, and *Su et al.*, 2014]. As emphasized by *Schwendike et al.* [2014], the same is true for the zonal overturning circulations in each ocean basin, usually referred to as the Walker circulation in the tropical Pacific. Importantly for the present work, trends in these averaged circulations will not generally be the same, or even have the same sign, as the local or regional-scale circulations. Hence, the question arises: how well do trends in the Hadley or Walker circulation represent local or regional trend? Answering this question is the main aim of the present paper. It is changes in these local- or regional-scale circulations that are directly linked to changes in local or regional-scale precipitation and hence potential societal impacts.

Although there is an accepted way of portraying the Hadley circulation, based on the zonally averaged mass stream function [e.g., *Hartmann*, 1994], there is no similar standard way of portraying the Walker circulation. The Walker circulation is commonly defined as the meridionally averaged overturning circulation over a restricted latitudinal band, and often confined to the tropical Pacific Ocean [e.g., *Julian and Chervin*, 1978; *Vecchi et al.*, 2006; *Power and Smith*, 2007; *Tokinaga et al.*, 2012].

One way of defining the local Hadley and local Walker circulations is by using a variation of the ψ vector method developed by *Keyser et al.* [1989]. This method uniquely and objectively partitions the divergent (irrotational) part of the three-dimensional flow into a pair of orthogonal two-dimensional circulations [*Schwendike et al.*, 2014]. Based on this method the present paper investigates how the local Hadley and local Walker circulations have changed between 1979 and 2009 in four reanalyses data sets. The advantage of the method is that it allows us to average over limited domains and to describe local Hadley and local Walker circulations in an unambiguous way.

The present study does not aim to address the sources for changes in the local Hadley and Walker circulations but aims to apply a new method to define the local Hadley and Walker circulations in order to analyze how these circulations have changed during the last 30 years in four modern-day reanalyses.

The remainder of the paper is structured as follows. The data and methodology used in this study are outlined in section 2. The annual and seasonal distributions of the mass flux and rainfall as well as their respective linear trends are discussed in section 3. Section 4 examines the local Hadley and Walker circulations and their trends. The meridionally and zonally averaged mass flux is discussed in sections 5 and 6, respectively. The relationship between the trends in both circulations and ENSO is discussed in section 7. The key conclusions are summarized in section 8.

2. Data and Method

A version of the ψ vector method, originally developed by *Keyser et al.* [1989], is used to decompose the tropical atmosphere into a pair of orthogonal overturning circulations which are the local Hadley and local Walker circulations. *Schwendike et al.* [2014] showed that after averaging over a restricted latitudinal band, part of the meridional overturning circulation (the Hadley circulation) is aliased into the definition of the Walker circulation. To avoid this problem, *Schwendike et al.* [2014] defined the Walker circulation as the meridional average of the local Walker circulation. This aliasing problem is potentially important when analyzing trends in the Walker circulation as these trends may be conflated with trends in the Hadley circulation. Likewise, the Hadley circulation was defined by *Schwendike et al.* [2014] as the zonal average of the local Hadley circulation, although averaging over a limited region introduces only small aliasing errors into the definition as the contribution from the zonal overturning circulation is generally small. This aliasing problem is particularly important when diagnosing changes in the Hadley and Walker circulations. Unless done correctly, taking the meridional average over a limited domain would attribute parts of the local Hadley circulation to the local Walker circulation [*Schwendike et al.*, 2014].

The ψ vector method is briefly summarized now; for more details see *Schwendike et al.* [2014]. The vector stream function $\boldsymbol{\psi}$ is defined as

$$\nabla_p \cdot \boldsymbol{\psi} = -\nabla_p^2 \mu = \omega, \tag{1}$$

where μ is a potential function, ∇_p is the gradient operator in isobaric coordinates, and ω is the vertical motion. The divergent wind can be written in terms of the velocity stream function as

$$\mathbf{u}_{\text{div}} = (u_\lambda, u_\phi) = -\frac{\partial \boldsymbol{\psi}}{\partial p} = -\left(\frac{\partial \psi_\lambda}{\partial p}, \frac{\partial \psi_\phi}{\partial p} \right), \tag{2}$$
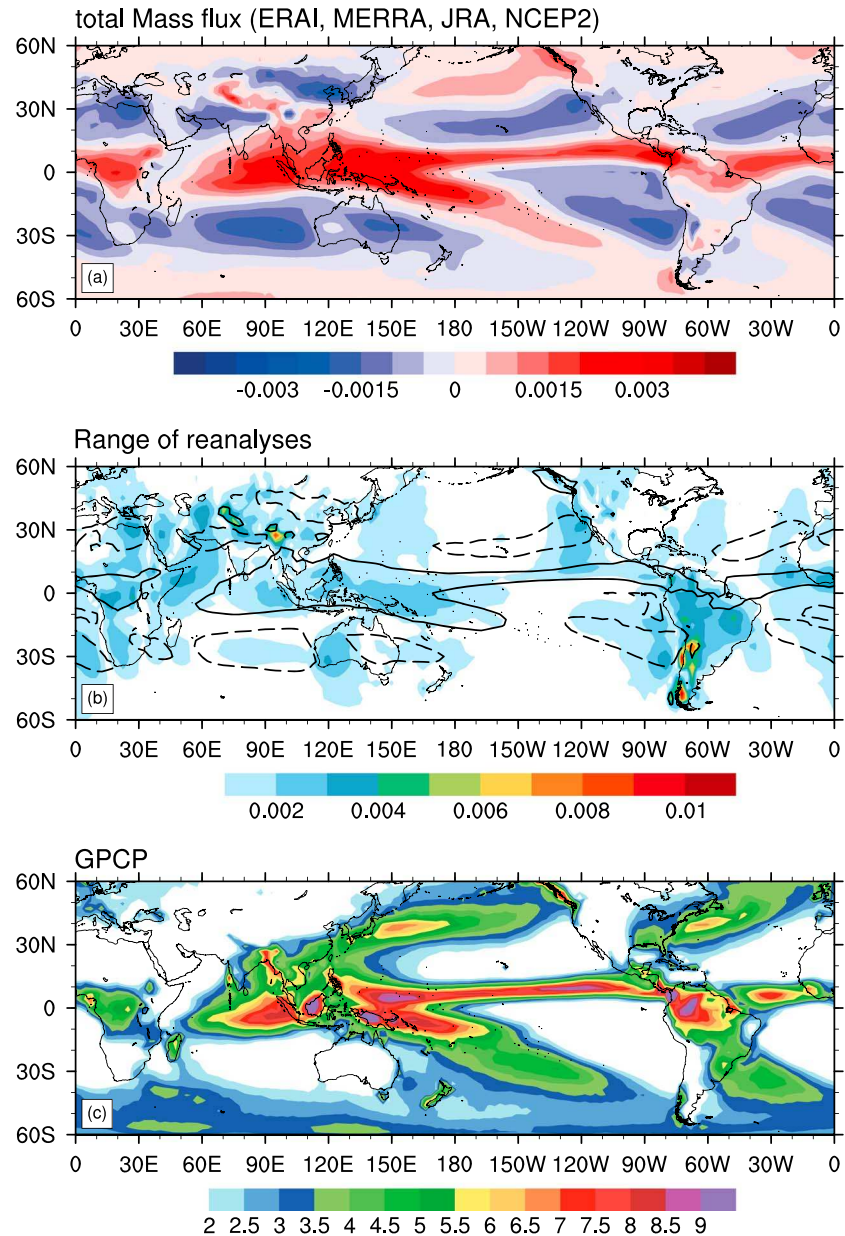
Figure 1. (a) The annual average of the total mass flux (kg m^{-2} s^{-1}) at 500 hPa averaged over ERAI, NCEP2, MERRA, and JRA reanalyses (1979–2009). (b) The range of the reanalyses (kg m^{-2} s^{-1}), calculated by subtracting the maximum from the minimum among the four reanalyses at each grid point. The solid black contour displays the annual mean total mass flux of +0.001 kg m^{-2} s^{-1} and the dashed black line the mean mass flux of −0.001 kg m^{-2} s^{-1} to illustrate the regions of ascent and descent. (c) The annual average of the GPCP precipitation (mm d^{-1}) between 1979 and 2009.

where u_λ and u_ϕ are the zonal and meridional components of the divergent part of the wind and ψ_λ and ψ_ϕ are the components of ψ in the zonal and meridional directions respectively. The vertical motion can be partitioned uniquely into the zonal and meridional planes as

$$\omega_\lambda \cos\phi = \frac{1}{a}\frac{\partial \psi_\lambda}{\partial \lambda} = \frac{1}{a^2 \cos\phi}\frac{\partial^2 \mu}{\partial \lambda^2}, \tag{3}$$

$$\omega_\phi \cos\phi = \frac{1}{a}\frac{\partial}{\partial \phi}(\psi_\phi \cos\phi) = \frac{1}{a^2}\frac{\partial}{\partial \phi}\left(\cos\phi \frac{\partial \mu}{\partial \phi}\right), \tag{4}$$
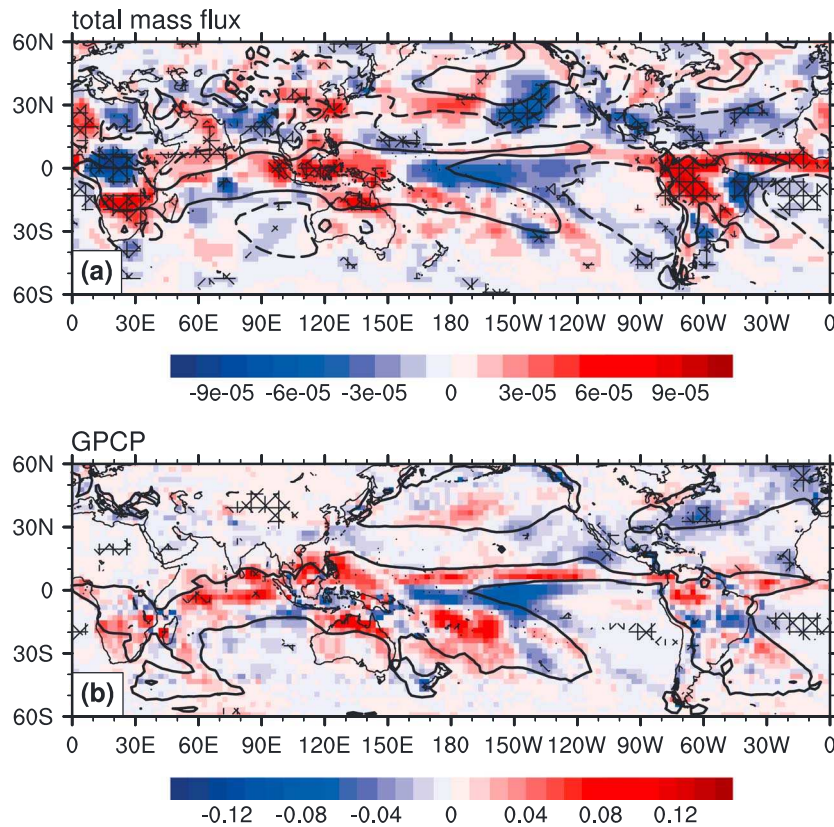
Figure 2. (a) The linear trend between 1979 and 2009 of the total mass flux (kg m^{-2} s^{-1} per 31 years) at 500 hPa based on the average of the mass flux in ERAI, NCEP2, MERRA, and JRA reanalyses for the season DJF. The contours of mean total mass flux of ± 0.001 kg m^{-2} s^{-1} illustrate the regions of ascent and descent. (b) The linear trend between 1979 and 2009 of the GPCP precipitation (mm d^{-1} per 31 years) for DJF. The mean precipitation of 3.0 mm d^{-1} is show in contours. The cross hatching in all plots highlights the regions where the linear trend has a statistical significance of 90% (based on Student's *t* test).

where *a* is the radius of the Earth. The vertical motion is the sum of the vertical motion partitioned in the two orthogonal directions $\omega = \omega_\lambda + \omega_\phi$. The upward mass fluxes associated with the zonal and meridional parts of the circulation are

$$m_\lambda = -\omega_\lambda \cos\phi/g \qquad \text{and} \qquad m_\phi = -\omega_\phi \cos\phi/g, \tag{5}$$

respectively, where *g* is the gravitational acceleration.

The meridional overturning circulation at a point or in a plane is the local Hadley circulation, and the zonal overturning circulation at a point or in a plane is the local Walker circulation. Both circulations satisfy continuity independently. In the present study the local Hadley circulation is portrayed by the stream function ψ_ϕ, the vertical mass flux m_ϕ, and the divergent part of the circulation in the meridional plane (u_ϕ, ω_ϕ). Likewise, the local Walker circulation is portrayed by the stream function ψ_λ, the vertical mass flux m_λ and the divergent circulation in the zonal plane $(u_\lambda, \omega_\lambda)$.

Our version of the ψ vector method is applied to four reanalyses in the period between 1979 and 2009: (i) The European Centre for Medium range Weather Forecasts ERA-Interim (ERAI) [*Simmons et al.*, 2011; *Dee et al.*, 2011], (ii) the National Centers for Environmental Prediction-Department of Energy reanalysis 2 data set (NCEP2) [*Kistler et al.*, 2001], (iii) the NASA Modern Era Retrospective analysis for Research and Applications (MERRA) [*Rienecker et al.*, 2011], and (iv) the Japanese Meteorological Agency 25 year reanalysis and climate data assimilation system (JRA) [*Onogi et al.*, 2007]. The ERAI data used is available at 6-hourly intervals at a horizontal resolution of 1.5°. The MERRA data set is available every 3 h at 1.25° horizontal resolution. Both NCEP2 and JRA reanalysis data are available at a horizontal resolution of 2.5° every 6 h. Each data set is interpolated to a common 2.5°× 2.5°horizontal grid for consistency.
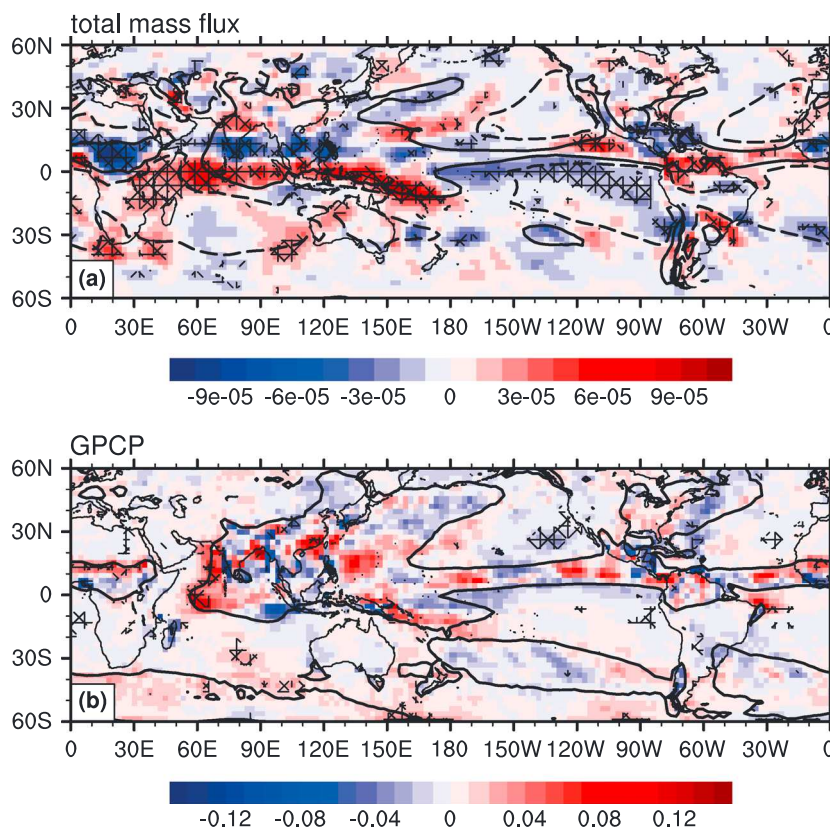
Figure 3. The same as Figure 2 but for JJA.

The Global Precipitation Climatology Project (GPCP) provides monthly mean precipitation data for the period 1979–2009, combining observations and satellite precipitation data on a 2.5°× 2.5°global grid [*Adler et al.*, 2003]. The data set used is the GPCP version 2.2 combined precipitation data provided by the National Oceanic and Atmospheric Administration (NOAA) / Ocean and Atmospheric Research (OAR) / Earth System Research Laboratory (ESRL) /Physical Science Division (PSD), Boulder, Colorado, USA.

3. Mass Flux and Rainfall

The annual average of the total mass flux, which is the sum of the zonal and meridional mass flux, at 500 hPa averaged over all four reanalyses is shown in Figure 1a. To quantify how the four renanalyses differ from each other, the difference between the maximum and the minimum value at each grid point is plotted (Figure 1b). The differences between the reanalyses are largest in the tropics, especially in the north of South America, the Maritime Continent, central Africa, over the Andes and the Himalayas. Nevertheless, the regions of upward mass flux largely coincide with the regions of precipitation (Figure 1b). Even though the individual reanalyses vary, their mean appears to give a consistent picture of the annual precipitation. The same conclusion holds for the seasonal means (not shown). This consistency check illustrates the close and expected relationship between the upward mass flux and precipitation.

The linear trend in total mass flux and GPCP precipitation for each season is calculated. In December, January, and February (DJF) over Africa there is a decrease in upward mass flux (Figure 2a) and precipitation (Figure 2b) near the equator and an increase south of it, indicating a southward shift of the circulation. These are also regions in which the statistical significance, calculated using the Student's *t* test, exceeds 90%. However, the trend in precipitation is weaker than the trend in mass flux, which might be due to changes in land surface [e.g., *Taylor et al.*, 2002]. Other factors, such as the horizontal advection of moisture, may also affect precipitation. Furthermore, there are positive trends in the vertical mass flux and precipitation over the Maritime Continent. The pattern over parts of the western and central Pacific shows a decrease along the equator and south of it, along with an increase in the mass flux and precipitation in the south west of that region, implying a southward shift of the circulation. The upward mass flux and precipitation increase over the northern part of
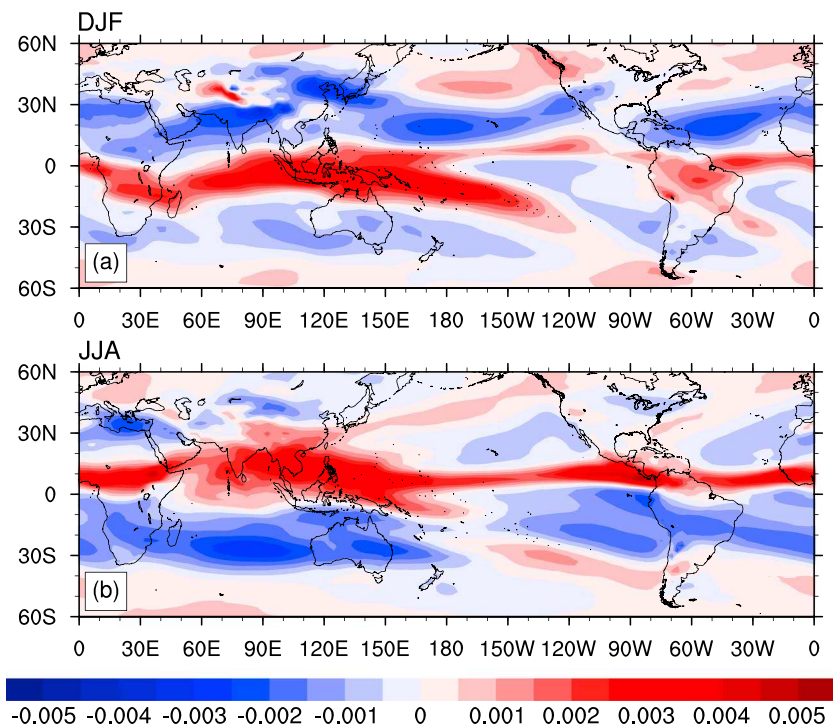
Figure 4. The local Hadley circulation. The meridional mass flux (kg m^{-2} s^{-1}) for the seasons (a) DJF and (b) JJA is shown in shadings of red (ascent) and blue (descent) at 500 hPa and are averaged over ERAI, NCEP2, MERRA, and JRA reanalyses (1979–2009).

South America and the equatorial Atlantic and decrease on the eastern and western flanks of these regions, implying a strengthening of the local overturning circulation.

In June, July, and August (JJA), the linear trend in total mass flux shifts southward of the region of upward and downward mass flux over Africa, the Indian Ocean, and the Maritime Continent (Figure 3a). This shift is partly reflected in the precipitation trend (Figure 3b), particularly in the western and central Pacific. There is an increase in mass flux over northern South America and only a slight (less than 0.04 mm d^{-1} over 31 years) increase in precipitation. In the eastern Pacific, roughly between 10 and 20°N and 100–130°W, there is an increase in upward mass flux (about 7×10^{-5} kg m^{-2} s^{-1} over 31 years) and a distinct increase in precipitation (about 0.08 mm d^{-1} over 31 years). The decrease in mass flux south of this region is distinct (about -8×10^{-5} kg m^{-2} s^{-1} and -0.12 K d^{-1} over 31 years, respectively), but less marked in the precipitation trend (about -0.03 mm d^{-1} over 31 years). In the Atlantic, there is an increase in upward mass flux along about 10°N (about 5×10^{-5} kg m^{-2} s^{-1} over 31 years) as well as in precipitation (about 0.08 mm d^{-1} over 31 years).

4. Local Hadley and Walker Circulations

The time-mean local Hadley (Figure 4) and local Walker (Figure 5) circulations are defined by the meridional and zonal mass fluxes at 500 hPa and are averaged over the four reanalyses. In both DJF and JJA, the local Hadley circulation (Figure 4) is characterized by zonally elongated bands of vertical mass flux, with marked ascent in the tropics and marked subsidence in the subtropics. The ascent is shifted toward the summer hemisphere, whereas the subsidence is more distinct in the winter hemisphere. In the equatorial eastern Pacific, however, there is subsidence along the equator, extending southward into the extratropics. North of this region, there is strong ascent marking the Intertropical Convergence Zone.

The bands of vertical mass flux comprising the time-mean local Walker circulation are mostly meridionally oriented (Figure 5). Almost everywhere, the time-mean local Walker circulation is weaker, and its seasonal variation is smaller, than the corresponding time-mean local Hadley circulation. In DJF, the time-mean local Walker circulation is most pronounced on the western sides on the Southern Hemisphere continents (Figure 5a) with ascent over the continents and subsidence over the adjacent oceans. The time-mean local Walker circulation is strongest over the eastern Pacific and South America. Similarly, there are pronounced bands of subsidence
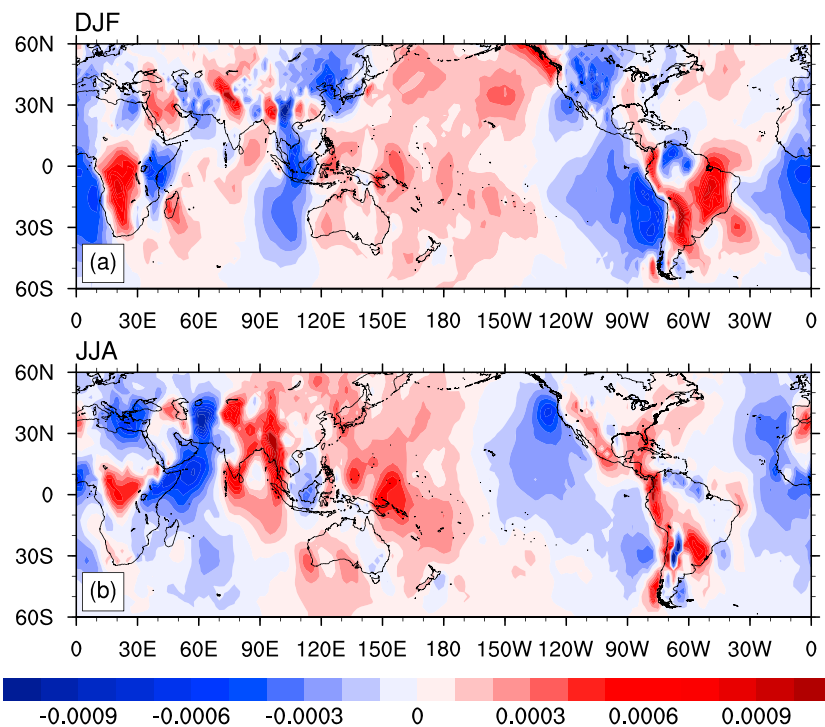
Figure 5. The local Walker circulation. The zonal mass flux (kg m^{-2} s^{-1}) for the seasons (a) DJF and (b) JJA is shown in shadings of red (ascent) and blue (descent) at 500 hPa and are averaged over ERAI, NCEP2, MERRA, and JRA reanalyses (1979–2009).

over the Atlantic and over the Indian Ocean to the west of Australia. These bands of subsidence are accompanied by ascent on the western side of southern Africa and western Australia. Patterns of alternating ascent and subsidence lie over the Rocky Mountains, the Middle East, and Asia and are most likely a consequence of the underlying orography.

In JJA, the time-mean local Walker circulation (Figure 5b) is more pronounced in the Northern Hemisphere. Ascent is centered on the Bay of Bengal and to its north, over the western Pacific, and through much of the Americas and the Caribbean. Notable centers of subsidence lie over the eastern Mediterranean Sea, over Somalia and the western Indian Ocean, to the east of the Caspian Sea, and off the west coast of the United States. Strong bands of ascent and subsidence lie along the Andes. These results are in good agreement with those in *Schwendike et al.* [2014], which are based only on the ERAI reanalysis.

The comparison of the meridional mass flux in each of the four reanalyses in DJF and JJA (Figure 6) shows that the local Hadley circulation has a similar strength and position in ERAI (Figures 6a and 6b) and in MERRA (Figures 6e and 6f). The local Hadley circulation in both reanalyses is stronger than in NCEP2 (Figures 6c and 6d) and in JRA (Figures 6g and 6 h), which are relatively similar. Even though the magnitude of the upward and downward mass flux varies over the four reanalyses used in the present study, the position of the regions of ascent and descent is the same and reflects the distribution shown in Figure 4.

Comparing the local Walker circulation in all four reanalyses shows, similar to the comparison for the local Hadley circulation, that distribution and strength of the zonal vertical mass flux is similar in ERAI (Figures 7a and 7b) and MERRA (Figures 7e and 7f) as well as in NCEP2 (Figures 7c and 7d) and JRA (Figures 7g and 7h). While there are differences between the reanalyses, the overall pattern is the same.

The linear trends for the local Hadley (Figure 8) and local Walker (Figure 9) circulations at 500 hPa show that the regional differences are large and changes in the magnitude of the vertical mass flux range from values between 1 and 10×10^{-5} kg m^{-2} s^{-1} over 31 years. Additionally, there is no coherent picture around the globe for either the local Hadley or the local Walker circulation.

In DJF, there is a weakening and a southward shift by about 1° degree over 31 years of the local Hadley circulation over Africa (Figure 8a). Over the Indian Ocean, a northward shift by about half a degree occurs, whereas
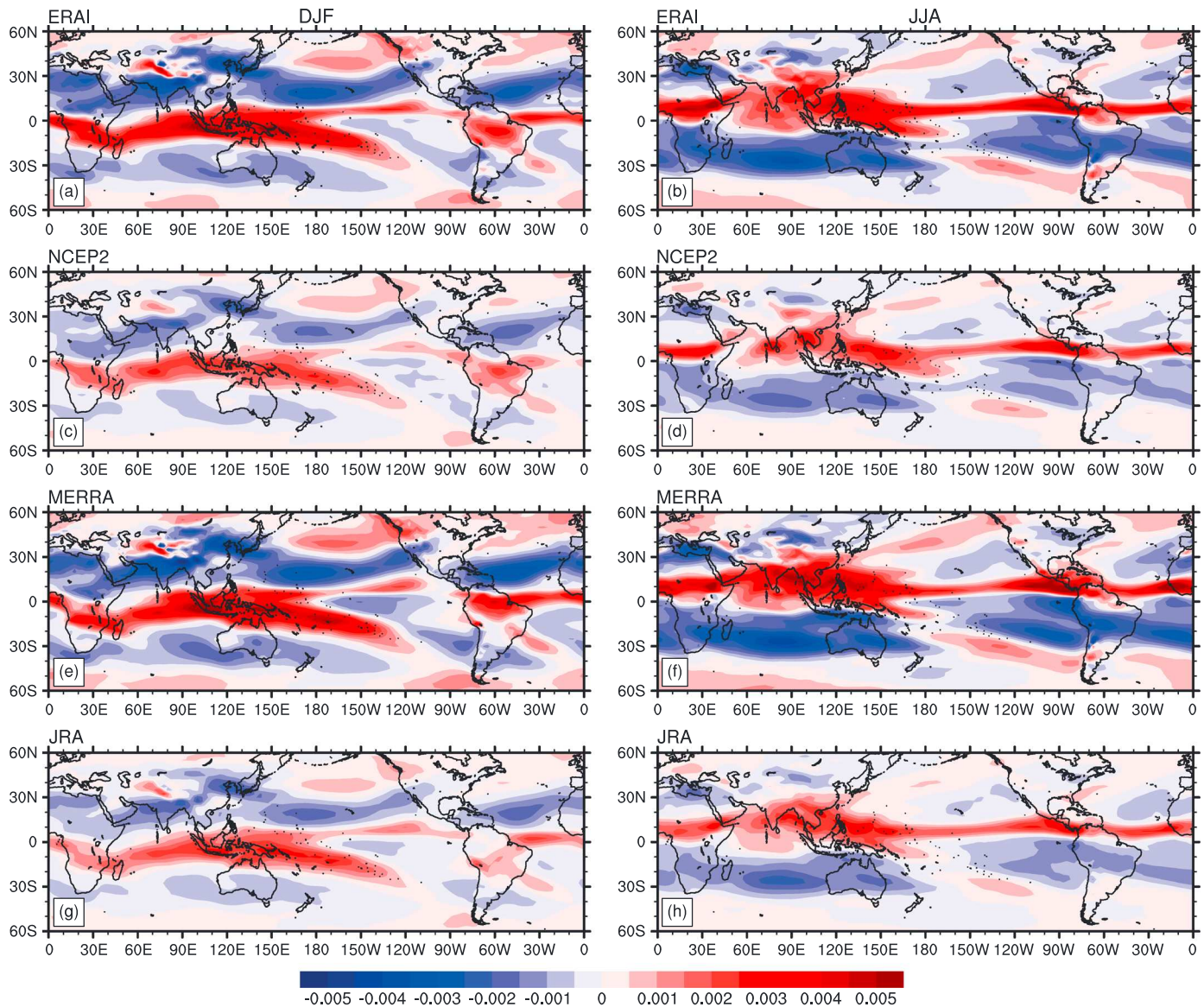
Figure 6. The meridional mass flux (kg m^{-2} s^{-1}) for the seasons DJF and JJA averaged over the period 1979–2009 are shown in shadings of red (ascent) and blue (descent) at 500 hPa for the reanalyses (a, b) ERAI, (c, d) NCEP2, (e, f) MERRA, and (g, h) JRA.

over the Maritime Continent the region of the upward mass flux increases more strongly than the downward mass flux leading to an enhancement of the local Hadley circulation. In contrast, over the western and central Pacific the local Hadley circulations are shifted toward the south by about 1° over 31 years. Over South America and the Caribbean as well as in the Atlantic the local Hadley circulations intensify (the upward mass flux increases by about 6×10^{-5} kg m^{-2} s^{-1} and the downward mass flux decreases by about -6×10^{-5} kg m^{-2} s^{-1} over 31 years). In JJA, the trends are very similar except that there is a southward shift in the local Hadley circulation all the way from Africa to the western Pacific by about half to 1° over 31 years (Figure 8b). The local Hadley circulation intensifies in the eastern Pacific, over South America, and in the Atlantic with an increase in upward mass flux by about 6×10^{-5} kg m^{-2} s^{-1} and a decrease in downward mass flux by about -6×10^{-5} kg m^{-2} s^{-1} (roughly by 1–5%) over 31 years. The pattern of the trends in the local Hadley circulation (Figures 8a and 8b) is very similar to that for the total mass flux (Figures 2a and 3a), emphasizing that the local Hadley circulation makes the larger contribution to the total mass flux.

The upward mass flux associated with the local Walker circulation over Africa and South America and the downward mass flux on either side intensifies in DJF (Figure 9a). Over parts of the Maritime Continent, along
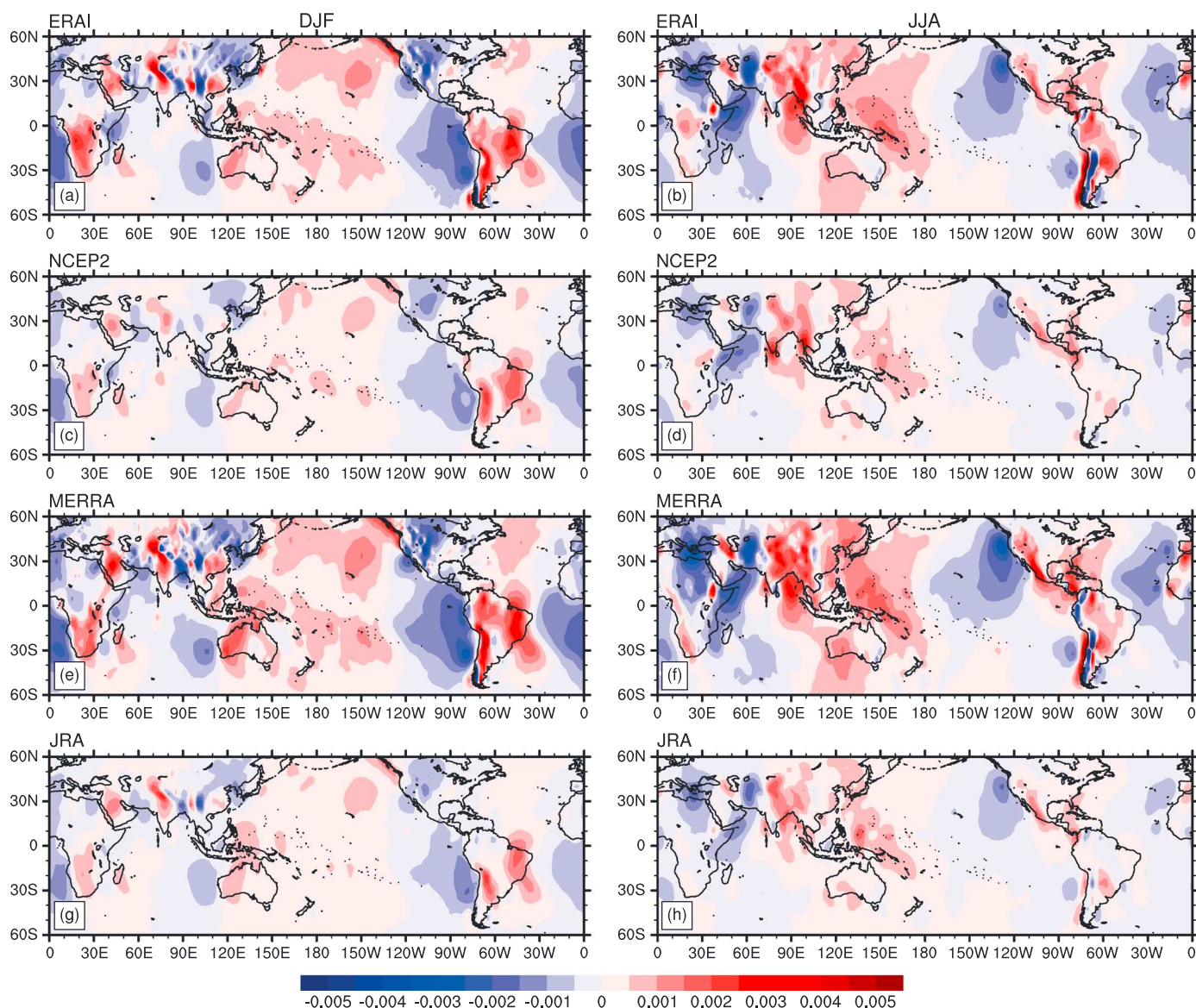
Figure 7. The zonal mass flux (kg m^{-2} s^{-1}) for the seasons DJF and JJA averaged over the period 1979–2009 are shown in shadings of red (ascent) and blue (descent) at 500 hPa for the reanalyses (a, b) ERAI, (c, d) NCEP2, (e, f) MERRA, and (g, h) JRA.

the coast of China and in the eastern Indian Ocean there is a band of increased, i.e., less negative, mass flux as well as decrease in mass flux over India and south of it. Hence, the local Walker circulation in the Indian Ocean as well as in the Atlantic Ocean weakens and shifts to the west. The pattern of the trends in the Pacific lacks a coherent structure and is characterized by a slight weakening (about -1×10^{-5} kg m^{-2} s^{-1} per 31 years) or no change in the local Walker circulation. The trend pattern in JJA (Figure 9b) is less pronounced but similar to that in DJF.

In both seasons the zonal mass flux increased over Africa, the Maritime Continent and South America and decreased by either side of it, both by about 10–20% in the mean over all reanalyses. Although the local Hadley circulation is stronger than the local Walker circulation in an absolute sense, the percentage changes in the local Walker circulation (not shown) are larger than in the local Hadley circulation.

As the local Hadley circulations are slightly different in all four reanalyses we expect the linear trend to be somewhat different too (Figure 10). In DJF, all reanalyses show an increase in mass flux in southern Africa and a decrease in equatorial Africa. This trend is weakest in NCEP2 (Figure 10c) and strongest in MERRA (Figure 10e). The signal in the linear trend in northern Africa is also similar in all reanalyses but differs in
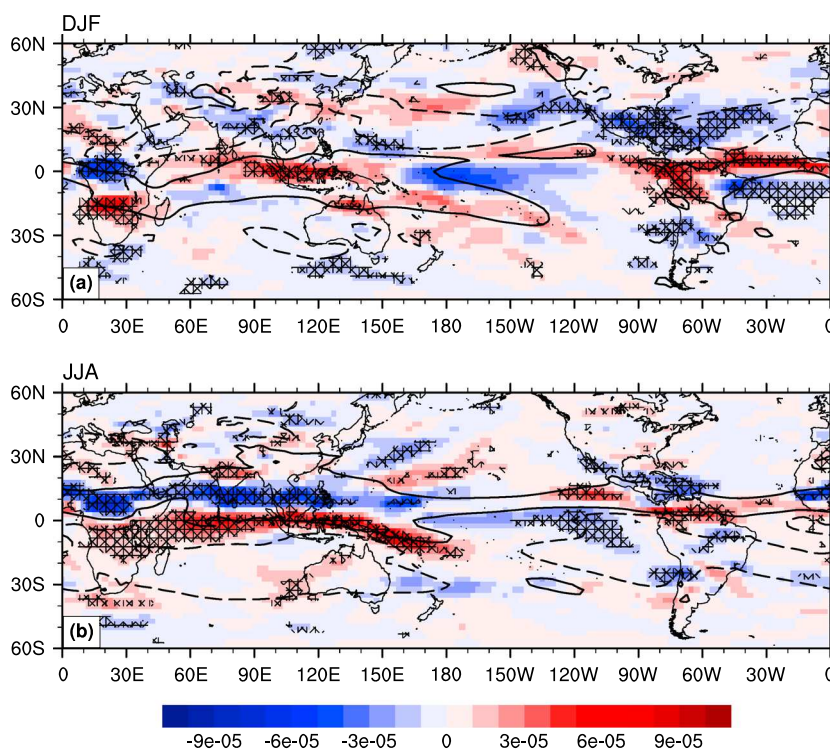
Figure 8. The linear trend between 1979 and 2009 at 500 hPa for the local Hadley circulation based on the average of meridional mass flux in the ERAI, NCEP2, MERRA, and JRA reanalyses. The trend in the mean meridional mass flux (kg m^{-2} s^{-1} per 31 years) for the seasons (a) DJF and (b) JJA is shown in shadings of red (increase) and blue (decrease). The contours of the mean meridional mass flux of ±0.001 kg m^{-2} s^{-1} illustrate the regions of ascent and descent in the 31 year mean. The cross hatching highlights the regions where the linear trend has a statistical significance of 90% (based on Student's t test).

strength, with the trend in MERRA being the largest. The zonally elongated band of increased mass flux across the Indian Ocean, the Maritime Continent, and the western Pacific varies somewhat in strength and position with the largest differences over the Indian Ocean and Australia. Over the Indian Ocean in ERAI (Figure 10a) and NCEP (Figure 10c), the vertical mass flux decreases in the region where ascent occurs in the 31 year mean, and increases north and south of this region, indicating a weakening of the local Hadley circulation. In MERRA (Figure 10e) the ascending branch of the local Hadley circulation is shifted northward and in JRA the meridional overturning circulation in the Indian Ocean is strengthened (Figure 10g). All reanalyses show the southwestward shift of the SPCZ, and an increase in vertical mass flux over the northern part of South America, and the equatorial Atlantic. The mass flux increases near the equator in the eastern Pacific in ERAI, MERRA, and JRA, whereas in NCEP2 descent can be found in the same region and the band of increased mass flux lies further north.

The linear trends in JJA show a consistent southward shift of the local Hadley circulation extending from Africa to the Maritime continent In NCEP2 (Figure 10d), MERRA (Figure 10f), and JRA (Figure 10)g. The trend pattern is different over the Indian Ocean in ERAI (Figure 10b), but similar over the Maritime Continent. All reanalyses show the southwestward shift in the South Pacific Convergence Zone (SPCZ) and the strengthening of the local Hadley circulation over South America and the Atlantic. In all reanalyses, but ERAI, the local Hadley circulation is also strengthened in the Eastern Pacific. Note, in all linear trends the regions with a statistical significance of 90% are very small and differ from reanalysis to reanalysis.

The linear trend in the local Walker circulation in all four reanalyses (Figure 11) shows an increase in vertical mass flux over the Maritime Continent and South America, and a decrease east and west of the continents. The vertical mass flux increased over parts of southern Africa in ERAI (Figure 11a), NCEP2 (Figure 11c), and JRA (Figure 11g), and decreased north, east, and west of this region. In MERRA (Figure 11e), however, the mass flux decreases over large parts of Africa and increases on either side. The signal is less clear over the oceans. In the eastern Pacific the downward mass flux is intensified in ERAI and JRA. All reanalyses show a decrease
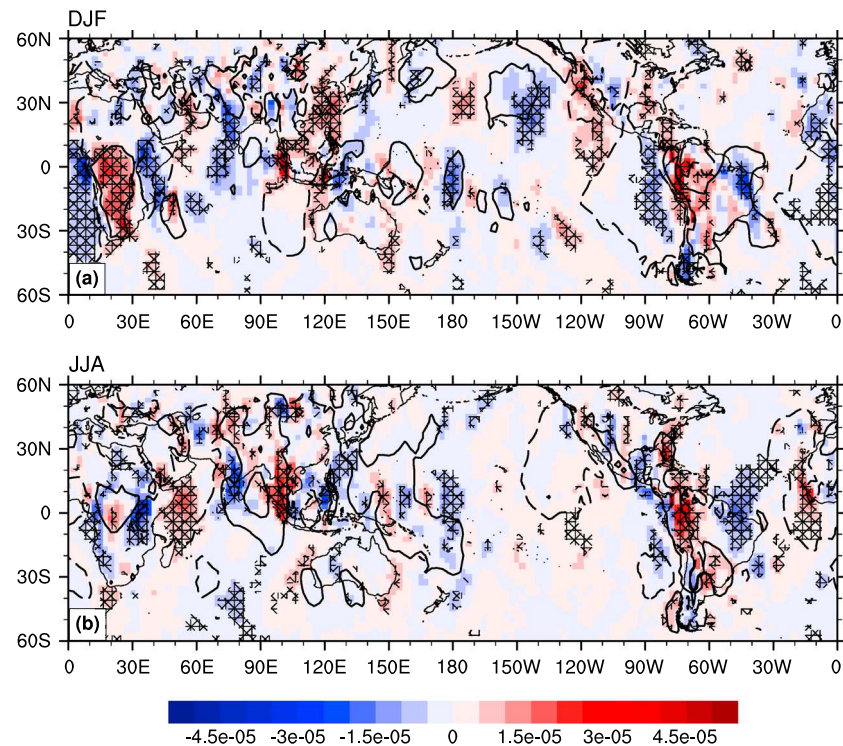
Figure 9. The linear trend between 1979 and 2009 at 500 hPa for the local Walker circulation based on the average the zonal mass flux in the ERAI, NCEP2, MERRA, and JRA reanalyses. The trend in the mean zonal mass flux (kg m^{-2} s^{-1} per 31 years) for the seasons (a) DJF and (b) JJA is shown. The contours of mean zonal mass flux of ± 0.002 kg m^{-2} s^{-1} illustrate the regions of ascent and descent in the 31 year mean. The cross hatching highlights the regions where the linear trend has a statistical significance of 90% (based on Student's t test).

in mass flux in the central Pacific and an increase over the Maritime Continent as mentioned earlier. In the Atlantic, the mass flux increases in ERAI and MERRA and near the equator in JRA, whereas it decreases slightly in NCEP2. All reanalyses show a pronounced decrease in the eastern Atlantic, indicating a weakening of the zonal overturning circulation. In the Indian Ocean, the trend pattern varies in all reanalyses. They have in common that the vertical mass flux decreases over India and the region south of it.

A westward shift in the local Walker circulations by on average about 1–2°in each ocean basin is evident in Figure 12). This is even more apparent when taking the vertical average between 900 and 200 hPa (not shown). For this analysis we portray the local Walker circulations by the zonal stream function ψ_λ. Taking the mean over DJF between 1979 and 2009 reveals a major cell in each ocean basin: one in the Pacific Ocean, one in the Indian Ocean, and one in the Atlantic Ocean (Figure 12a). The difference in ψ_λ between 1995–2009 and 1979–1994 shows a decrease from 130° to 180°E and an increase from 80° to 120°E, indicating a shift in the Walker circulation to the west. There is an increase in ψ_λ in the longitudinal band 120°–70°W, and another in the band 30°W–30°E. Areas of decrease occur between 30°–70°E and 60°–40°W, showing that the local Walker circulations in each basin is shifted westward. This shift to the west is largest in the Pacific and Indian Oceans, being about 4–5° over 31 years between 80°E–140°W and 1–2° in the eastern Pacific.

In JJA, the three overturning cells over each ocean basin are present in the meridionally averaged zonal stream function (Figure 12b), although their position is different to that in DJF. The center of each cell is shifted to the west, and the cell in the Indian Ocean is stronger than in DJF. The difference between 1995–2009 and 1979–1994 reveals areas of decrease between about 60°E–150°W and 60°–40°W, and areas of increase between 110°–70°W and 30°W–40°E. These changes imply that the local Walker circulation in the Pacific Ocean and in the Indian Ocean is shifted to the west. This westward shift is most distinct in the Pacific and over the Maritime Continent with the shift being 1–2°. In the other regions the local Walker circulation shifts only by about 1° or less. The local Walker circulation in the Atlantic mainly weakens.
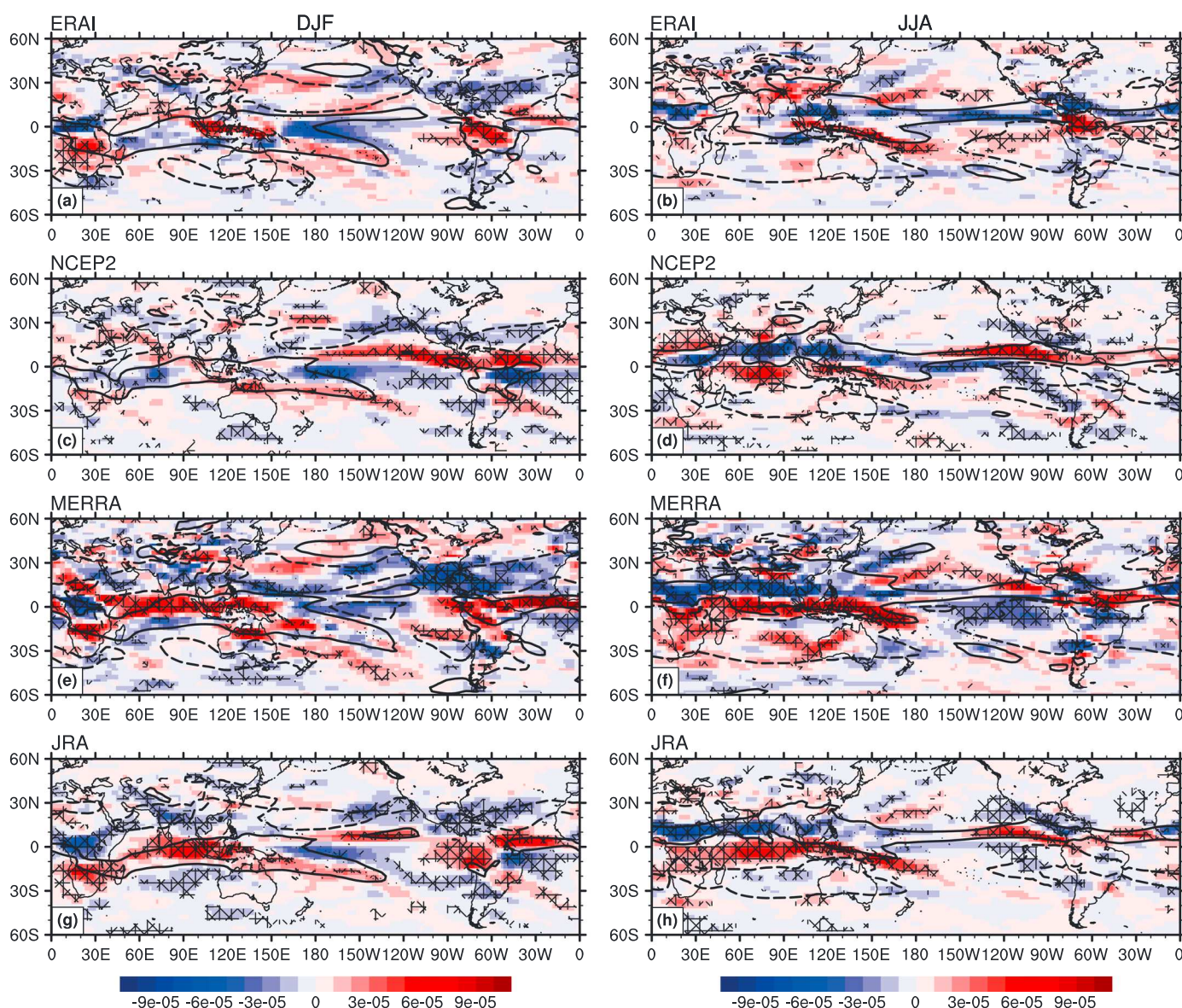
Figure 10. The linear trend between 1979 and 2009 at 500 hPa for the local Hadley circulation based on the meridional mass flux in the (a, b) ERAI, (c, d) NCEP2, (e, f) MERRA, and (g, h) JRA reanalyses. The trend in the meridional mass flux (kg m^{-2} s^{-1} per 31 years) for the seasons DJF and JJA is shown in shadings of red (increase) and blue (decrease). The contours of the meridional mass flux of ± 0.001 kg m^{-2} s^{-1} illustrate the regions of ascent and descent in the 31 year mean. The cross hatching highlights the regions where the linear trend has a statistical significance of 90% (based on Student's t test).

5. Zonally Averaged Mass Flux

The Hovmöller plot for the Hadley circulation (not the local Hadley circulation) at 500 hPa for DJF and JJA, zonally averaged around the whole globe (0–360°E), is shown in Figure 13. Note, the zonal average around the whole globe over the meridional mass flux gives the standard view of the Hadley circulation [*Schwendike et al.*, 2014]. The time on the ordinate ranges from 1979 to 2009 and the latitude is given on the abscissa. During the Southern Hemisphere summer, the strongest mean downward mass flux lies in the Northern Hemisphere subtropics between about 10°N to 35°N, with weaker mean downward mass flux in the Southern Hemisphere, poleward of 30°S (Figure 13a). The ascending branch of the Hadley circulation straddles the equator, albeit displaced toward the Southern Hemisphere (Figure 13a). To the extent that the ascending branch can be considered a single region of ascent from, say, 10°N to 20°S, the Hadley circulation comprises a single cell during DJF. This is the conventional view, derived principally from the calculation of a mass-weighted stream function [e.g., *Hartmann*, 1994].
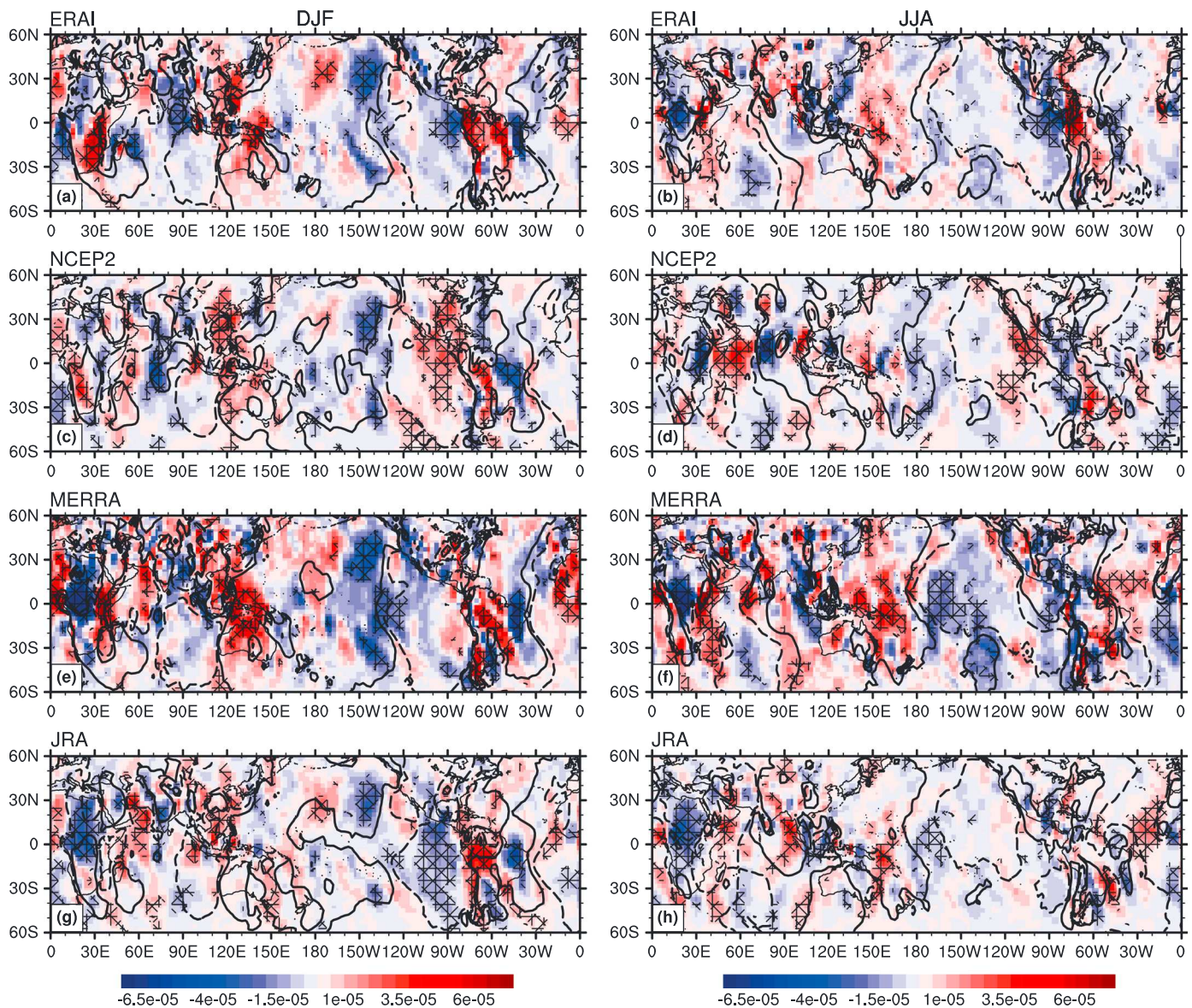
Figure 11. The linear trend between 1979 and 2009 at 500 hPa for the local Walker circulation based on the zonal mass flux in the (a, b) ERAI, (c, d) NCEP2, (e, f) MERRA, and (g, h) JRA reanalyses. The trend in the zonal mass flux (kg m^{-2} s^{-1} per 31 years) for the seasons DJF and JJA is shown. The contours of zonal mass flux of ± 0.002 kg m^{-2} s^{-1} illustrate the regions of ascent and descent in the 31 year mean. The cross hatching highlights the regions where the linear trend has a statistical significance of 90% (based on Student's t test).

During the Northern Hemisphere summer, the Hadley circulation is characterized unequivocally as a single overturning cell (Figure 13b). There is a band of strong mean upward mass flux in the Northern Hemisphere tropics, accompanied by a band of strong mean downward mass flux in the Southern Hemisphere.

The linear trend shows that the upward mass flux between the equator and 10° N increases strongly at a rate 1.5×10^{-5} kg m^{-2} s^{-1} over 31 years in DJF (Figure 13e). Likewise, the region of downward mass flux during DJF in the Northern Hemisphere strengthens (meaning it becomes more negative) at the rate of 0.9×10^{-5} kg m^{-2} s^{-1} over 31 years. Taken together, these results imply a strengthening of the Northern Hemisphere winter cell, in agreement with previous work on the topic [see *Quan et al.*, 2004, and the references therein]. However, the upward mass flux decreases in the band 10° south of the equator, and increases slightly poleward of that region, indicating a weakening and southward shift of the Southern Hemisphere summer cell.

The upward mass flux in the summer hemisphere in JJA (5°N–20°N) decreases strongly at a rate of 1.8×10^{-5} kg m^{-2} s^{-1} over 31 years (Figure 13f). On either side of this region, however, the mass flux increases,
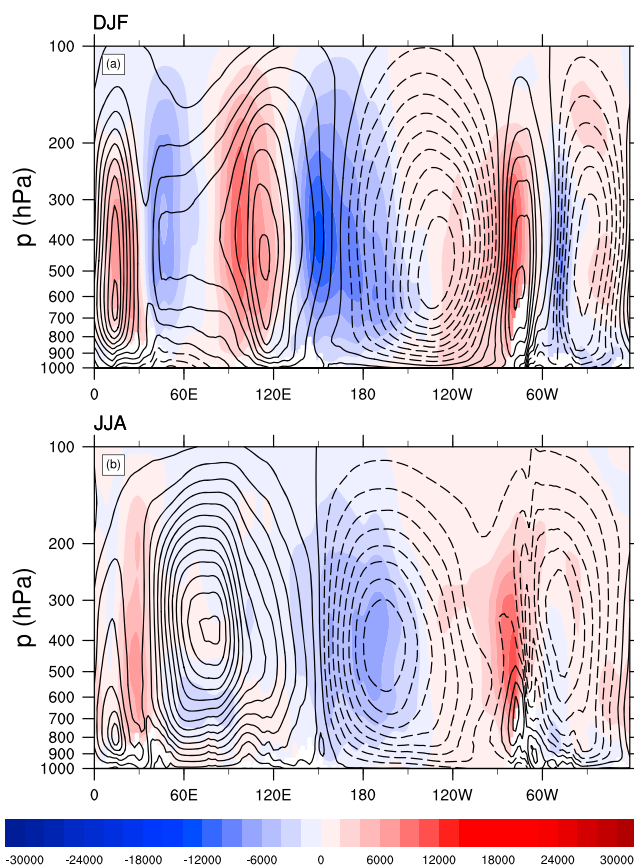
Figure 12. The difference of the zonal stream function ψ_λ between (1995–2009) and (1979–1994) for the seasons (a) DJF and (b) JJA shaded, and the position of the mean zonal stream function over 1979–2009 in contours. Both are averaged between 35°S and 10°N and are based on ERAI reanalysis data.

resulting in a weakening and widening of the Hadley circulation. The magnitude of the downward mass flux between about 5°S–20°S decreases, i.e., the mass flux becomes less negative, in agreement with the overall weakening of the Hadley circulation.

6. Meridionally Averaged Mass Flux

Figure 14 shows the meridional mean of the zonal part of the vertical mass flux at 500 hPa for DJF and JJA from 1979 to 2009, where the meridional average is taken from 35°S to 10°N. This latitudinal band is chosen as the largest zonal vertical mass flux occurs there (see Figure 5). This field represents the Walker circulation, although the definition is different from those used in past studies. During DJF, the Walker circulation comprises six distinct bands of vertical mass flux with alternating sign (or three distinct overturning cells; Figure 14a). The first is a narrow band of mean downward mass flux over the eastern Indian Ocean and southeast Asia (90°–110°E). This band shows strong variability and a slight weakening over the period (meaning the subsidence is reduced). This weakening can be seen in linear trend in this region which shows an increase in vertical mass flux, i.e., a reduction in downward mass flux (Figure 14c).

The second is a broad band of mean upward mass flux over the center of the Maritime Continent and the western and central Pacific (120°E–140°W), while the third is a band of mean downward mass flux over the eastern Pacific and central and north America (140°–80°W). The fourth band shows mean upward mass flux over South America and the western Atlantic (80°–40°W). The fifth is a band of mean downward mass flux lying over the eastern Atlantic and Africa (20°W–15°E). The final band is a mean upward mass flux over the eastern portion of Africa, as well as the western and central Indian Ocean (15°–90°E). This band is highly variable, with periods of downward mass flux embedded within.
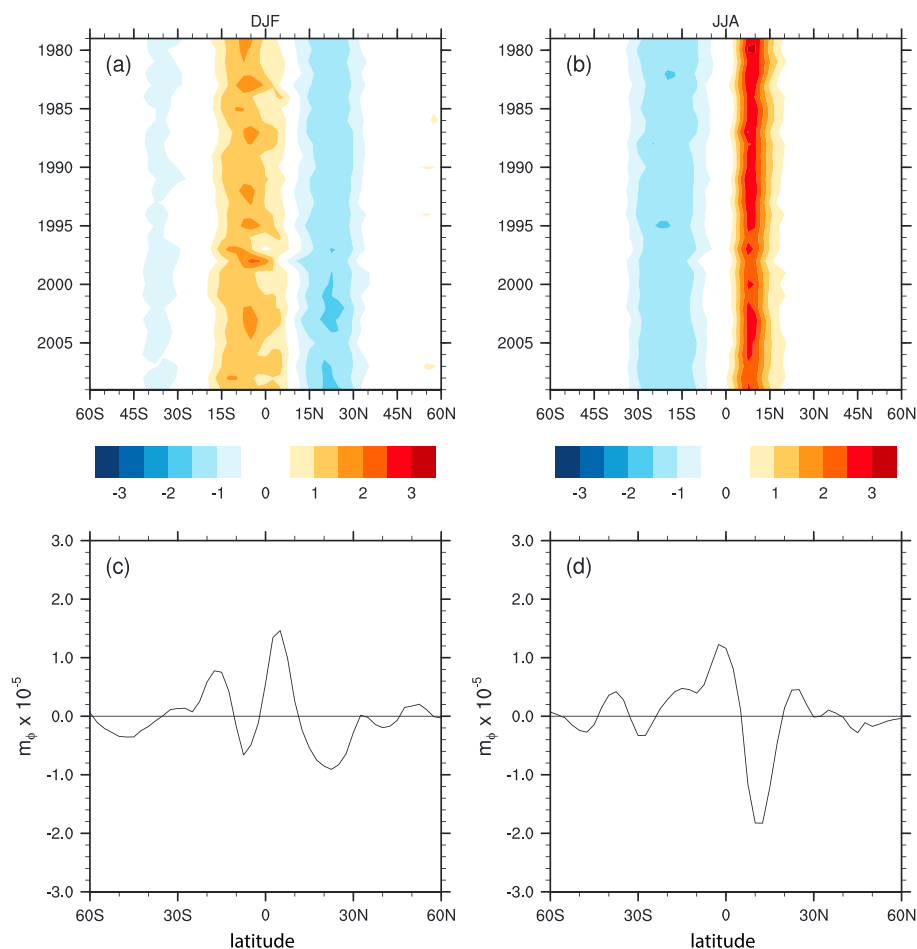
Figure 13. (a, b) The zonally averaged (0–360°) meridional vertical mass flux at 500 hPa averaged over ERAI, NCEP2, MERRA, and JRA reanalyses between 1979 and 2009 ($\times 10^{-3}$ kg m^{-2} s^{-1}) for the seasons DJF and JJA. (c, d) The averaged trend in the zonally averaged meridional mass flux ($\times 10^{-5}$ kg m^{-2} s^{-1} over 31 years).

The mass flux increases up to about 1.5×10^{-5} kg m^{-2} s^{-1} over 31 years between (10°–30°E) and (80°–40°W) (Figure 14c). East of 120°E the mass flux increases and west of 120°E the mass flux decreases, indicating a westward shift by about 4–5° in this region. Overall, the changes in vertical mass flux in the Pacific region are small and of varying sign. These results show that over the South America, the Atlantic, and Africa, the zonal part of the vertical mass flux has strengthened during DJF in the period 1979 to 2009.

In contrast, the number of distinct bands of vertical mass flux comprising the Walker circulation is less clear during JJA (Figure 14b) as the vertical mass flux in the band 30°–110°E changes sign. The first band, comprising mean downward mass flux lies from 30°W–15°E. Between 30°W and the Greenwich Meridian the vertical mass flux increases, i.e., it becomes less negative, and it becomes more strongly negative from 10°W to 10°E (Figure 14d). The second is a band of mean upward mass flux from 15° to 30°E, which increases particularly toward the end of the period 1979–2009. However, around 30°E the mass flux decreases by about -1.1×10^{-5} kg m^{-2} s^{-1} over 31 years. The third band is characterized by mean downward mass flux and ranges from 30°–80°E. In this band the mass flux weakens with time (becomes less negative). The fourth band of mean upward mass flux lies from 80°E to 160°W, and is made up of two, relatively distinct maxima, one centered over around 100°E and associated with the Asian monsoon, the other centered around 170°E in the western Pacific. The linear trend over this broad band changes sign frequently, but the upward mass flux in the region of the main maxima increases. The fifth is a band of mean downward mass flux from 170°–80°W, which mainly weakens. The sixth is a weak band of mean upward mass flux from 80°–50°W, which both strengthens from 80° to 60°W and weakens eastward of this region.

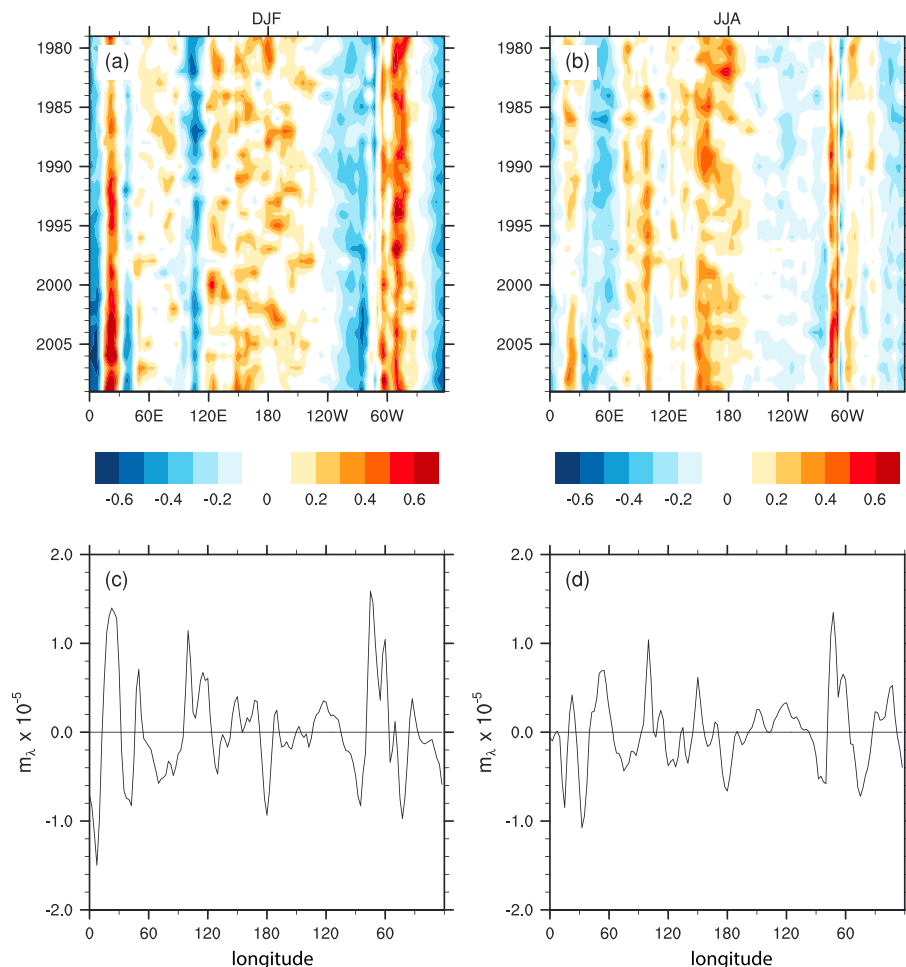**Figure 14.** The meridionally averaged (10°N–35°S) zonal vertical mass flux at 500 hPa averaged over ERAI, NCEP2, MERRA, and JRA reanalyses between 1979 and 2009 ($\times 10^{-3}$ kg m^{-2} s^{-1}) for the seasons (a) DJF and (b) JJA. (c, d) The averaged trend in zonal mass flux ($\times 10^{-5}$ kg m^{-2} s^{-1} over 31 years).

7. The Effect of ENSO on the Trends

As ENSO is the largest mode of variability in the tropics it is important to investigate in what way (if any) trends in ENSO affect the calculated trends in the local Hadley and Walker circulations described in the previous sections.

To analyze changes during the two phases of ENSO, the differences in the local Hadley and Walker circulations in La Niña and El Niño periods are computed. The El Niño events are defined by a monthly Southern Oscillation Index (SOI) less than −0.9 standard deviation, whereas La Niña events are defined by an SOI larger than 0.9 standard deviation. The anomalies for the annual total mass flux (Figure 15a) and GPCP rainfall (Figure 15b) show much the same pattern as each other. There are large positive anomalies in the western and central Pacific and in the central southern Pacific, emphasizing the regions of enhanced convection during El Niño events. Over the Maritime Continent and along the South Pacific Convergence Zone (SPCZ) there is a distinct negative anomaly due to the shift of upward mass flux from the central Pacific to the Maritime continent between El Niño and La Niña periods [e.g., *Rasmusson and Carpenter*, 1982]. Partitioning the vertical mass flux into that associated with the local Hadley circulation (Figure 15c) and that associated with the local Walker circulation (Figure 15d) shows that the largest effect of ENSO is on the local Hadley circulation. The anomalies in the local Hadley circulation display a similar pattern to the anomalies in the total mass flux and precipitation, as El Niño is driven by a tongue of warm sea surface temperatures along the equator. Consequently, the meridional gradients are larger than the zonal gradients, and, hence, the response in meridional direction is stronger. As a result the local Hadley circulation is stronger than the local Walker circulation. Nonetheless, the

local Walker circulation strengthens during La Niña and weakens during El Niño. By construction, the sum of the local Hadley circulation and the local Walker circulation is the total mass flux.

To check whether there is a trend in the reanalyses related to a trend in ENSO, the monthly SOI time series, as well as its 5 month running mean, and their linear trends are plotted in Figure 16a. Also plotted in Figure 16b are the monthly NINO3.4 index and its 5 month running mean. None of the time series has a statistically significant trend. Only the SOI time series show any trends and they are well below the threshold for El Niño and La Niña events.

As an additional test of whether any analyzed trends can be attributed to trends in ENSO two new indices are defined based on the zonal and meridional mass fluxes; these indices are termed M_λ and M_ϕ, respectively. The definition of the M_λ follows the definition of the SOI, which is the standardized anomaly of the mean sea level pressure difference between Tahiti and Darwin. However, instead of choosing two points, two regions are selected. Region 1 lies over the Maritime Continent (125–135°E, 5°S–5°N) and region 2 is located in the central Pacific (165–155°W, 5°S–5°N). The zonal mass flux at 500 hPa is averaged over both regions, and their difference is taken (region 1 − region 2). This is done for each months. M_λ is then defined as the difference between the monthly difference between both regions, and the 31 year average of this months.

By analogy with the definition of the NINO3.4 index, a box in the central Pacific (170°E–140°W, 5°S–5°N) is chosen to represent the local Hadley circulation. M_ϕ is defined at 500 hPa as the difference between the monthly average and the 31 year average over the box.

The 5 month running mean of the indices M_λ and M_ϕ for each reanalysis as well as the average over all reanalyses are shown in Figures 16c and 16d, respectively. The SOI and the mean M_λ time series are highly correlated, the correlation coefficient being 0.83. The time series from ERAI has the highest correlation with the SOI. The linear trend in the mean time series of M_λ shows no statistically significant trend. Although the time series from MERRA shows a trend, which can be attributed to the relatively high start and end values of this time series, it is still within one standard deviation. The mean M_ϕ and the NINO3.4 are also highly correlated with a correlation coefficient of 0.91. Again, the time series from ERAI has the highest individual correlation with a small negative linear trend which is well below the threshold values for ENSO events.

The analysis above shows that there is no significant trend due to ENSO in any of the four reanalyses and that none of the trends analyzed in the previous section are related to changes in ENSO. Moreover, M_λ, which is a measure of the local Walker circulation in the Pacific, shows little trend. Likewise, M_ϕ, which expresses the strength of the mass flux within a box along the equatorial Pacific, shows no change in the last 31 years.

8. Conclusions

In this study a variation of the ψ vector method developed by *Keyser et al.* [1989] is used to uniquely partition the flow at 500 hPa from four reanalyses (ERAI, NCEP2, MERRA, and JRA) in to local Hadley and local Walker circulations. Further, linear trends for the local Hadley and local Walker circulations are calculated.

Patterns in the linear trends of the total mass flux and GPCP precipitation are similar in all seasons. In DJF the trend shows a fairly consistent southward shift in mass flux and precipitation over Africa, over the Maritime Continent, and over the northern part of South America. In JJA, the trends in the total mass flux and precipitation show a southward shift ranging from Africa to the central Pacific. Over northern South America and in the Atlantic, the mass flux and precipitation increase.

A key advantage of our decomposition method is that it allows a regional study of changes in Hadley and Walker circulations. We found there is no coherent global picture in the changes in both the local Hadley and the local Walker circulation. In addition, there are marked differences from season to season.

In DJF, the local Hadley circulation over Africa, the Maritime Continent, and the western and central Pacific has shifted southward by about 1° over 31 years and has strengthened by about 1–5% over the South America, the Caribbean and in the Atlantic. In JJA, the local Hadley circulation has shifted southward by about 0.5 to 1° over 31 years in the whole band from Africa to the western Pacific and has strengthened by about 1–5% over South and middle America and in the eastern Pacific.

The local Walker circulation is weaker than the local Hadley circulation in an absolute sense, but the percentage changes in the local Walker circulation are stronger than the changes in the local Hadley circulation.
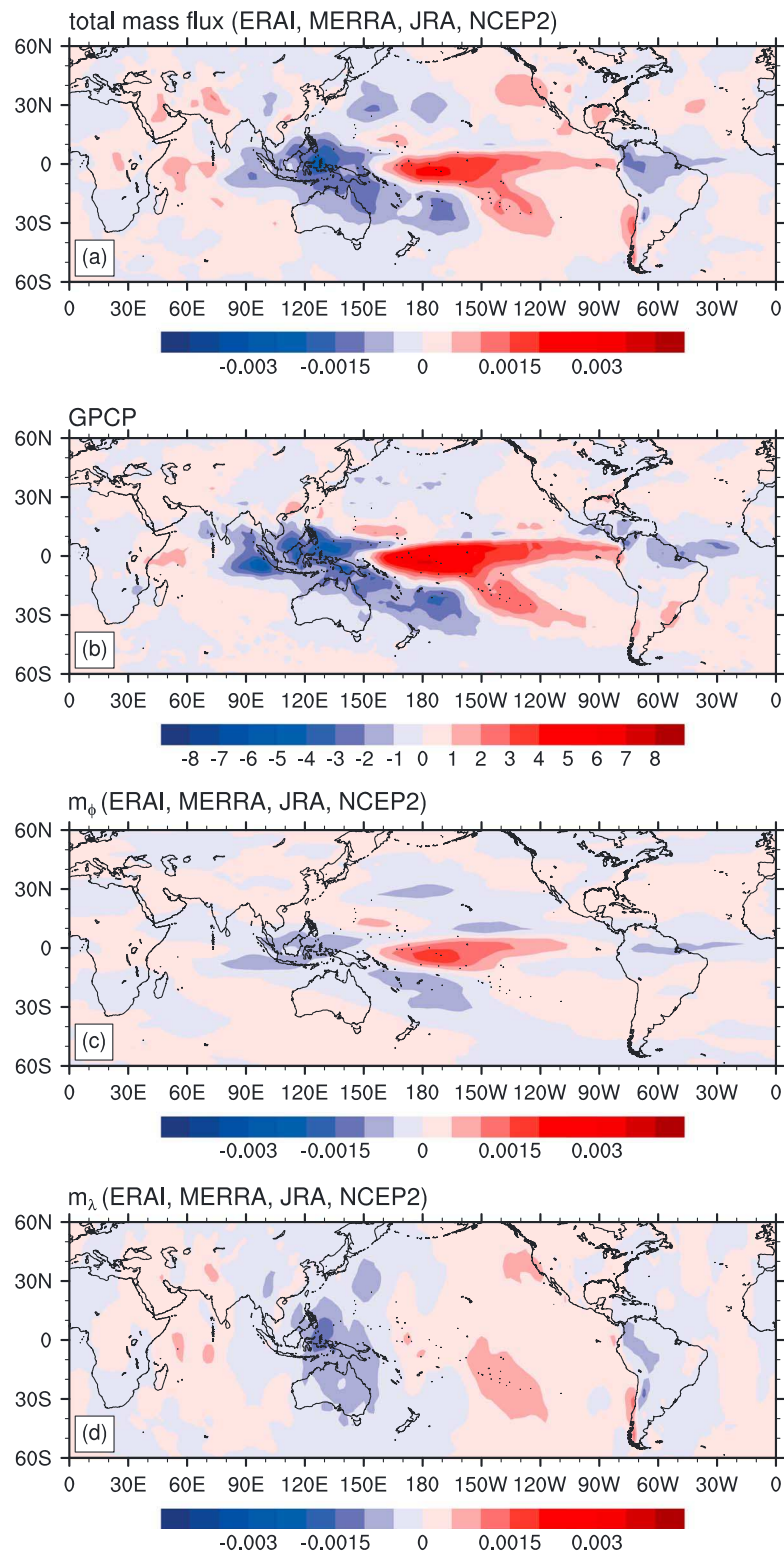
total mass flux (ERAI, MERRA, JRA, NCEP2)

GPCP

m_ϕ (ERAI, MERRA, JRA, NCEP2)

m_λ (ERAI, MERRA, JRA, NCEP2)

Figure 15. Differences between El Niño and La Niña. (a) The annual average of the total mass flux (kg m^{-2} s^{-1}) at 500 hPa averaged over ERAI, NCEP2, MERRA, and JRA reanalyses (1979–2009). (b) The annual average of the GPCP precipitation (mm d^{-1}) between 1979 and 2009. (c) The annual average of the mass flux in meridional direction (kg m^{-2} s^{-1}) at 500 hPa averaged over ERAI, NCEP2, MERRA, and JRA reanalyses (1979–2009). (d) The annual average of the mass flux in zonal direction (kg m^{-2} s^{-1}) at 500 hPa averaged over ERAI, NCEP2, MERRA, and JRA reanalyses (1979–2009).
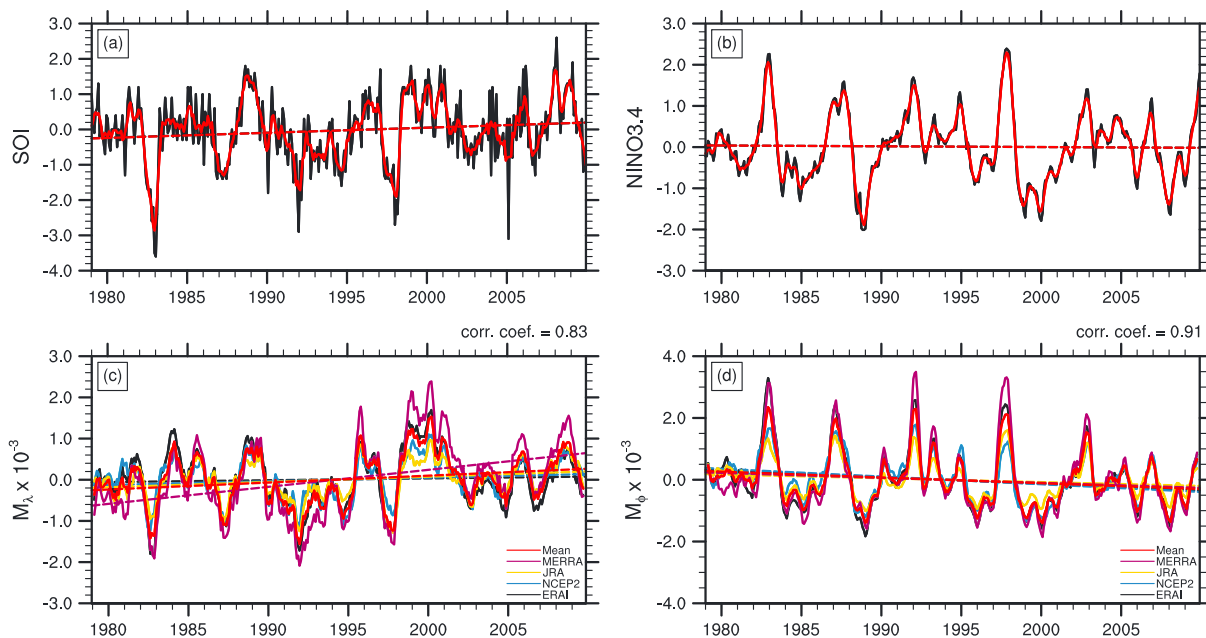
Figure 16. (a) Time series for the monthly SOI (black) and the 5 months running mean of the SOI (red). (b) Time series for the monthly NINO3.4 (black) and the 5 months running mean of the NINO3.4 index (red). (c) Time series of the 5 months running mean of the index M_λ for ERAI (black), NCEP2 (blue), JRA (yellow), MERRA (purple), and the average over all four reanalyses (mean in red). The correlation coefficient between the 5 months running mean of the SOI and the 5 months running mean of the mean of the M_λ is shown in correlation coefficient is in top right corner of Figure 16c. (d) Time series of the 5 months running mean of the new index M_ϕ for ERAI (black), NCEP2 (blue), JRA (yellow), MERRA (purple), and the average over all four reanalyses (mean in red). The correlation coefficient between the 5 months running mean of the NINO3.4 and the 5 months running mean of the mean M_ϕ, averaged over the four reanalyses, is shown in correlation coefficient is in top right corner of Figure 16d. Details on the new indices M_λ and M_ϕ can be found in section 7.

In both seasons, the local Walker circulations in the Indian Ocean and the Atlantic Ocean have weakened, whereas the local Walker circulation has changed little in the Pacific Ocean. The zonal mass flux has increased by about 10–20% over Africa, the Maritime Continent, and South America, and decreased by the about the same amount on either side of it. In only relatively small regions are the linear trends statistically significant at the 90% confidence level, although some of the largest changes (mass flux larger than 4×10^{-5} kg m^{-2} s^{-1} or smaller than -4×10^{-5} kg m^{-2} s^{-1} per 31 years) occur in these statistically significant regions.

This paper provides a new way to look at the trends in the local Hadley and local Walker circulations and shows that those changes vary greatly around the globe. Furthermore, there is general agreement in the sign and geographical pattern of the trends among the four reanalyses examined here. Although the regions where the trends are statistically significant are small, the results indicate that a more regional treatment of circulation changes is required if we are to understand the effect of climate variability and changes on the major tropical circulation systems. Applying the ψ vector method provides a useful first step in that direction. The next step is to investigate what causes these changes in the local Hadley and local Walker circulation.

References

Adler, R. F., et al. (2003), The version 2 Global Recipitation Climatology Project (GPCP) monthly precipitation analysis (1979-Present), *J. Hydrometeor.*, 4, 1147–1167.

Allen, R. J., S. C. Sherwood, J. R. Norris, and C. S. Zender (2012), Recent Northern Hemisphere tropical expansion primarily driven by black carbon and tropospheric ozone, *Nature*, 485, 350–354.

Bayr, T., D. Dommenget, T. Martin, and S. B. Power (2014), The eastward shift of the Walker circulation in response to global warming and its relationship to ENSO variability, *Clim. Dyn.*, 43, 2747–2763, doi:10.1007/s00382-014-2091-y.

Chen, J., B. Carlson, and A. Genio (2002), Evidence for strengthening of the tropical general circulation in the 1990s, *Science*, 296, 838–841.

Chen, S., K. Wei, W. Chen, and L. Song (2014), Regional changes in the annual mean Hadley circulation in recent decades, *J. Geophys. Res. Atmos*, 119, 7815–7832, doi:10.1002/2014JD021540.

Davis, S. M., and T. Birner (2013), Seasonal to multidecadal variability of the width of the tropical belt, *J. Geophys. Res. Atmos.*, 118, 7773–7787, doi:10.1002/jgrd.50610.

Davis, S. M., and K. H. Rosenlof (2012), A multi-diagnostic intercomparison of tropical width time series using reanalyses and satellite observations, *J. Clim.*, 25, 1061–1078.

Dee, D. P., et al. (2011), The ERA-Interim reanalysis: Configuration and performance of the data assimilation system, *Q. J. R. Meteorol. Soc.*, 137, 553–597.

Deser, C., and A. S. Phillips (2009), Atmospheric circulation trends, 1950–2000: The relative roles of sea surface temperature forcing and direct atmospheric radiative forcing, *J. Clim.*, *22*, 396–413.

DiNezio, P. N., G. A. Vecchi, and A. C. Clement (2013), Detectability of changes in the Walker circulation in response to global warming, *J. Clim.*, *26*, 4038–4048.

Fu, Q., and P. Lin (2011), Poleward shift of subtropical jets inferred from satellite-observed lower stratospheric temperatures, *J. Clim.*, *24*, 5597–5603.

Fu, Q., C. M. Johanson, J. M. Wallace, and T. Reichler (2006), Enhanced mid-latitude tropospheric warming in satellite measurements, *Science*, *312*, 1179, doi:10.1126/science.1125566.

Gastineau, G., H. Le Treut, and L. Li (2008), Hadley circulation changes under global warming conditions indicated by coupled climate models, *Tellus*, *60*, 863–884.

Gastineau, G., L. Li, and H. Le Treut (2009), The Hadley and Walker circulation changes in global warming conditions described by idealized atmospheric simulations, *J. Clim.*, *22*, 3993–4013.

Gedney, N., and P. J. Valdes (2000), The effect of Amazonian deforestation on the Northern Hemisphere circulation and climate, *Geophys. Res. Lett.*, *27*, 3053–3056.

Goswami, B. N., V. Krisnamurthy, and H. Annamalai (1999), A broadscale index for the interannual variability of the Indian summer monsoon, *Q. J. R. Meteorol. Soc.*, *125*, 611–633.

Hartmann, D. (1994), *Global Physical Climatology*, 411 pp., Acad. Press, New York.

Held, I. M., and B. J. Soden (2006), Robust responses of the hydrological cycle to global warming, *J. Clim.*, *19*, 5686–5699.

Hu, Y., and Q. Fu (2007), Observed poleward expansion of the Hadley circulation since 1979, *Atmos. Chem. Phys.*, *7*, 5229–5236.

Hu, Y., and Q. Fu (2013), Poleward expansion of the Hadley circulation in CMIP5 simulations, *Adv. Atmos. Sci.*, *30*, 790–795.

Johanson, C., and Q. Fu (2009), Hadley cell widening: Model simulations versus observations, *J. Clim.*, *22*, 2713–2725.

Julian, P. R., and R. M. Chervin (1978), A study of the Southern Oscillation and the Walker circulation phenomenon, *Mon. Weather Rev.*, *106*, 1433–1451.

Keyser, D., B. D. Schmidt, and D. G. Duffy (1989), A technique for representing three-dimensional vertical circulations in baroclinic disturbance, *Mon. Weather Rev.*, *117*, 2463–2494.

Kistler, R., et al. (2001), The NCEP-NCAR 50-year reanalysis: Monthly means CD-ROM and documentation, *Bull. Am. Meteorol. Soc.*, *82*, 247–267.

Liu, J., M. Song, and X. Ren (2012), Changes in the strength and width of the Hadley circulation since 1871, *Clim. Past*, *8*, 1169–1175.

Lu, J., G. A. Vecchi, and T. Reichler (2007), Expansion of the Hadley cell under global warming, *Geophy. Res. Lett.*, *34*, L06805, doi:10.1029/2006GL028443.

Lucas, C., B. Timbal, and H. Nguyen (2013), The expanding tropics: A critical assessment of the observational and modeling studies, *WIREs Clim.Change*, *5*, 89–112, doi:10.1002/wcc.251.

Nguyen, H., A. Evans, C. Lucas, I. Smith, and B. Timbal (2013), The Hadley circulation in reanalyses: Climatology, variability, and changes, *J. Clim.*, *26*, 3357–3376.

Onogi, K., et al. (2007), The JRA-25 reanalysis, *J. Meteorol. Soc. Jpn.*, *85*, 369–432.

Power, S., and I. Smith (2007), Weakening of the Walker Circulation and apparent dominance of El-Nino both reach record levels, but has ENSO really changed, *Geophy. Res. Lett.*, *34*, L18702, doi:10.1029/2007GL030854.

Quan, X., H. Diaz, and M. Hoerling (2004), Changes in the tropical Hadley cell since 1950, in *The Hadley Circulation: Present, Past and Future*, edited by H. F. Diaz and R. S. Bradley, chap. 3, pp. 85–120, Kluwer Acad. Publ., Netherlands.

Quan, X.-W., M. P. Hoerling, J. Perlwitz, H. F. Diaz, and T. Xu (2014), How fast are the tropics expanding?, *J. Clim.*, *27*, 1999–2013.

Rasmusson, E. M., and T. H. Carpenter (1982), Variations in tropical sea surface temperature and \emph{}surface wind fields associated with the Southern Oscillation/El Niño, *Mon. Weather Rev.*, *110*, 354–384.

Rienecker, M. M., et al. (2011), MERRA: NASA's modern-era retrospective analysis for research and applications, *J. Clim.*, *24*, 3624–3648.

Schwendike, J., P. Govekar, M. J. Reeder, R. Wardle, G. J. Berry, and C. Jakob (2014), Local Partitioning of the overturning circulation in the tropics and the connection to the Hadley and Walker circulations, *J. Geophys. Res. Atmos.*, *119*, 1322–1339, doi:10.1002/2013JD020742.

Seidel, D., and W. Randel (2007), Recent widening of the tropical belt: Evidence from tropopause observations, *J. Geophys. Res.*, *112*, D20113, doi:10.1029/2007JD008861.

Seidel, D., Q. Fu, W. Randel, and T. Reichler (2008), Widening of the tropical belt in a changing climate, *Nat. Geosci.*, *1*, 21–24.

Simmons, A., S. Uppala, D. Dee, and S. Kobayashi (2011), New ECMWF reanalysis products from 1989 onwards, *ECMWF Newslett.*, *110*, 26–35.

Stachnik, J. P., and C. Schumacher (2011), A comparison of the Hadley circulation in modern reanalyses, *J. Geophys. Res.*, *116*, D22102, doi:10.1029/2011JD016677.

Su, H., J. H. Jiang, C. Zhai, T. J. Shen, J. D. Neelin, G. L. Stephens, and L. Y. Yung (2014), Weakening and strengthening structures in the Hadley circulation change under global warming and implications for cloud response and climate sensitivity, *J. Geophs. Res. Atmos.*, *119*, 5787–5805, doi:10.1002/2014JD021642.

Tanaka, H., N. Ishizaki, and A. Kitoh (2004), Trend and interannual variability of Walker, monsoon and Hadley circulations defined by velocity potential in the upper troposphere, *Tellus*, *56*, 250–269.

Taylor, C. M., E. F. Lambin, N. Stephenne, R. J. Harding, and R. J. Essery (2002), The influence of land use change on climate in the Sahel, *J. Clim.*, *15*, 3615–3629.

Tokinaga, H., S.-P. Xie, C. Deser, Y. Kosaka, and Y. M. Okumura (2012), Slowdown of the Walker circulation driven by tropical Indo-Pacific warming, *Nature*, *491*, 439–443.

Vecchi, G., and B. Soden (2007), Increased tropical Atlantic wind shear in model projections of global warming, *Geophys. Res. Let.*, *34*, L08702, doi:10.1029/2006GL028905.

Vecchi, G., B. Soden, A. Wittenberg, I. Held, A. Leetmaa, and M. Harrison (2006), Weakening of tropical Pacific atmospheric circulation due to anthropogenic forcing, *Nature*, *441*, 73–76.